Direct Evidence for the Interaction of Stigmatellin with a Protonated Acidic Group in the bc_1 Complex from *Saccharomyces cerevisiae* As Monitored by FTIR Difference Spectroscopy and ^{13}C Specific Labeling†

Michaela Ritter,‡ Hildur Palsdottir,§ Masato Abe,|| Werner Mäntele,‡ Carola Hunte,§ Hideto Miyoshi,|| and Petra Hellwig*,‡

Institut für Biophysik, Johann Wolfgang Goethe-Universität, Theodor-Stern-Kai 7, Haus 74, 60590 Frankfurt am Main, Germany, Max-Planck-Institut für Biophysik, Marie-Curie Strasse 15, 60439 Frankfurt am Main, Germany, and Division of Applied Life Sciences, Graduate School of Agriculture, Kyoto University, Sakyo-ku, Kyoto 606-8502, Japan

Received February 17, 2004; Revised Manuscript Received April 21, 2004

ABSTRACT: In this study a combined electrochemical and FTIR spectroscopic approach was applied to monitor the binding of stigmatellin, a Q_o site inhibitor of the cytochrome bc_1 complex from *Saccharomyces cerevisiae*. Natural stigmatellin A induced clear shifts in the redox-induced FTIR difference spectra. For data interpretation a stigmatellin derivative (UST) with the conjugated trienes replaced by an aliphatic tail was synthesized, and the carbonyl group shown in crystal structures to interact with His181, the [2Fe-2S] ligand of the Rieske, was specifically ^{13}C labeled. Electrochemically induced FTIR difference spectra of the inhibitors in CH_3OD were obtained and revealed signals characteristic for the oxidized and reduced forms of the labeled and unlabeled compounds. On the basis of signals from the inhibitors alone, the binding of the inhibitor to the bc_1 complex was monitored. Direct evidence for the interaction of the carbonyl group with the protein was provided by the observed shift of the ν(C═O) vibrational mode of about 10 cm^{-1}. In addition, redox-dependent reorganizations of the protein were identified, including protonation changes of acidic residues at 1746 and 1734 cm^{-1}. The conformational changes observed upon inhibitor binding are discussed with respect to the crystal structures and proposed mechanistic models [Hunte, C., Koepke, J., Lange, C., Rossmanith, T., and Michel, H. (2000) *Structure 8*, 669−684; Palsdottir, H., Lojero, C. G., Trumpower, B. L., and Hunte, C. (2003) *J. Biol. Chem. 278*, 31303−31311].

The cytochrome bc_1 complex[1] (ubiquinol−cytochrome *c* oxidoreductase; complex III) is one of the fundamental components of the respiratory electron transfer chains located in the inner mitochondrial or bacterial cytoplasmic membranes (*1*). The enzyme catalyzes the electron transfer from ubiquinol to cytochrome *c*, which is coupled to translocation of protons across the membrane. All bc_1 complexes contain three catalytic subunits: cytochrome *b* with two *b*-type hemes (heme b_L and b_H), cytochrome c_1 with a covalently bound *c*-type heme, and the Rieske iron−sulfur protein with an [2Fe-2S] cluster (ISP). Mitochondrial complexes have up to eight additional subunits, and for *Saccharomyces cerevisiae* seven additional subunits are known. The structures of bc_1 complexes from bovine (*3*, *5*), chicken (*4*), and yeast (*2*) mitochondria have been determined by X-ray crystallography, and the 2.3 Å resolution structure of the yeast complex has the highest resolution available so far (*2*).

The catalytic mechanism of the bc_1 complex is described with the protonmotive Q cycle (*6*−*8*). Key features include two separate substrate binding sites for ubiquinol and ubiquinone, called the Q_o site (quinol oxidation site, near heme b_L) and Q_i site (quinone reduction site, near heme b_H). The Q cycle operates in two identical half-reactions, in which altogether two quinols are oxidized to quinone at the Q_o site. Each quinol oxidation reaction releases two electrons, which undergo a bifurcated reaction. One electron is transferred via the ISP and cytochrome c_1 to reduce cytochrome *c*, while the other is transferred to the Q_i site via heme b_L and heme b_H. Two cycles of quinol oxidation are therefore needed to fully reduce quinone to quinol, via a semiquinone intermediate. A main feature of the Q cycle is the net translocation of protons across the membrane against a concentration gradient, where two protons are consumed by quinone reduction and four protons are released by quinol oxidation, therefore contributing to the electrochemical proton gradient which drives ATP synthesis. Although the Q cycle is well understood, the molecular details and regulatory events in quinol oxidation are not clear. Especially, the mechanisms behind

† This work is supported by the Deutsche Forschungsgemeinschaft (SFB 472) to C.H., P.H., and W.M., the Max-Planck Gesellschaft (scholarship to H.P.) ,and a Grant-in-Aid for Scientific Research from the Japan Society for the Promotion of Science (Grant 15380083 to H.M.).

* To whom correspondence should be addressed. E-mail: hellwig@biophysik.uni-frankfurt.de. Phone: +49-69-6301-4227. Fax: +49-69-6301-5838.

‡ Johann Wolfgang Goethe-Universität.

§ Max-Planck-Institut für Biophysik.

|| Kyoto University.

[1] Abbreviations: IR, infrared; FTIR, Fourier transform infrared; UV/vis, ultraviolet/visible; bc_1 complex, ubiquinol−cytochrome *c* oxidoreductase; b_H, high-potential *b*-type heme; b_L, low-potential *b*-type heme; Q_o, ubiquinol oxidation site; Q_i, ubiquinone reduction site; SHE′, standard hydrogen electrode (for pH 7); UM, *n*-undecyl β-D-maltoside; UST, undecylstigmatellin.

10.1021/bi049649x CCC: $27.50
Published on Web 06/09/2004

the bifurcated electron flow and different models of Q_o site occupancy provoke discussion (*9*−*13*).

Inhibitors provide an important tool to analyze the molecular mechanism of the bc_1 complex and have been extensively used to characterize the different quinone binding sites (see, for example, ref *30*). Depending on their binding properties, Q_i and Q_o site-specific inhibitors have been distinguished. Inhibitors binding at the Q_o site are further classified into three subgroups: Q_o-I inhibitors (e.g., myxothiazol, MOA-stilbene) bind to the proximal domain of the bilobal Q_o site and affect the spectroscopic properties of heme b_L, Q_o-II inhibitors (like HDBT) bind to the distal domain and affect the EPR line shape of the Rieske [2Fe-2S] cluster, and Q_o-III inhibitors (stigmatellin) show interaction with the Rieske protein and influence the heme b_L spectral properties.

The crystal structure of the bc_1 complex with natural stigmatellin A bound at the Q_o site showed tight and specific binding of the inhibitor. The position of the conjugated trienes is stabilized by several van der Waals interactions with cytochrome *b* residues. The chromone headgroup is stabilized by numerous nonpolar and a few polar interactions, including a hydrogen bond from the carbonyl group (4-C═O) to His181, one of the [2Fe-2S] cluster ligands of the Rieske protein, which is thereby fixed in docking position on cytochrome *b* (*2*). On the heme b_L facing side of the inhibitor the 8-hydroxy group is within hydrogen bond distance to the side chain of cytochrome *b* residue Glu272. Binding of stigmatellin was discussed to mimic that of an intermediate of ubiquinol oxidation (*2*). On the basis of the structures and biochemical characterization of variants, Glu272 was proposed to be part of the proton exit pathway for ubiquinol oxidation (*2*, *30*, *33*, *35*).

Reaction-induced FTIR difference spectroscopy is a sensitive method to detect even subtle structural changes taking place upon the redox reactions of the enzyme. In this study we combined FTIR difference spectroscopy and isotope labeling of a modified Q_o site inhibitor, stigmatellin (Q_o-III), to monitor the conformational changes of the protein upon inhibitor binding and identify redox-dependent alterations in the protonation state of acidic residues.

Redox-induced FTIR difference spectroscopy has already been applied to investigate several different membrane proteins (*14*−*16*) and was recently applied to extract information about bacterial (*14*, *17*) and mitochondrial bc_1 complexes (*18*). Here, we present for the first time the redox-induced difference FTIR analysis of the bc_1 complex from the yeast *S. cerevisiae*, with a substrate analogue bound at the Q_o site, and discuss the functional consequences of this study with respect to mechanistic models based on X-ray structures (*2*, *33*).

MATERIALS AND METHODS

Synthesis of Undecylstigmatellin and ^{13}C-Labeled Undecylstigmatellin. The synthetic procedures of unlabeled and ^{13}C-labeled undecylstigmatellin (UST) are schematically shown in Figure 1C. Benzopyran-4-one structure was constructed as described (*31*). Specific ^{13}C labeling at the 4-position of benzopyran-4-one ring was achieved by introduction of a propionyl group using a propionic-*1*-^{13}*C* acid (99 atom % ^{13}C, Aldrich) in reaction step a. Structures of UST and ^{13}C-UST were characterized by ^{1}H NMR and

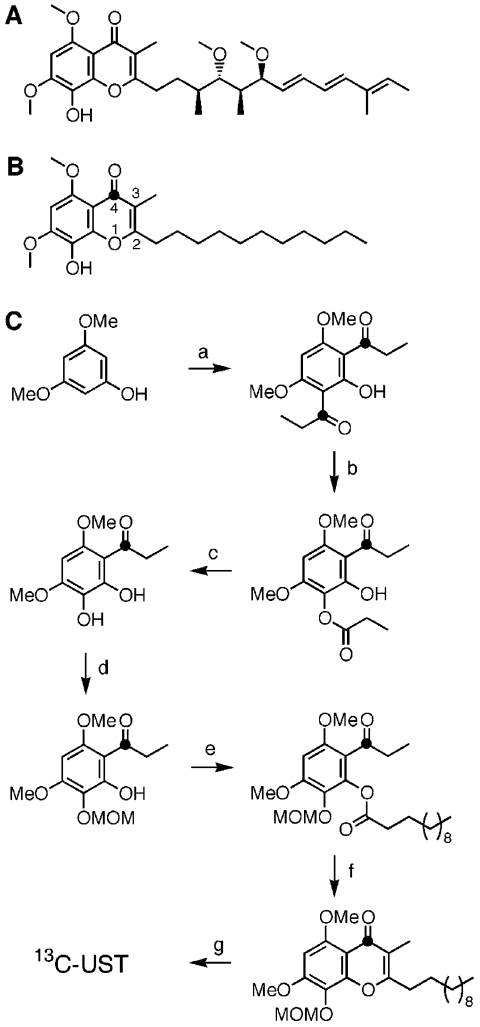

FIGURE 1: Structures of natural stigmatellin A (A) and [4-^{13}C]-undecylstigmatellin (UST) (B). A black dot indicates the position of the ^{13}C label. Synthetic procedures of UST and [4-^{13}C]UST are shown in (C). Reaction conditions: (a) propionic acid (or propionic-*1*-^{13}*C* acid), P_4O_{10}, H_3PO_4, 70 °C; (b) TFA, *m*-CPBA, CH_2Cl_2, 4 °C; (c) MeOH, HCl, reflux; (d) MOMCl, $(i\text{-Pr})_2$NEt, CH_2Cl_2, room temperature; (e) dodecanoyl chloride, $(i\text{-Pr})_2$NEt, 4-(dimethylamino)pyridine, CH_2Cl_2, room temperature; (f) MeOH, Na, reflux; (g) 4% AcCl in MeOH, room temperature.

MS spectra. The ^{13}C enrichment of the 4-position was confirmed by the split 3-methyl proton signal ($^3J_{C-H}$ = 3.6 Hz). UST: ^{1}H NMR (300 MHz, $CDCl_3$) δ 0.88 (t, J = 6.5 Hz, 3H), 1.21−1.42 (m, 16H), 1.73 (tt, J = 7.5, 7.5 Hz, 2H), 2.00 (s, 3H), 2.67 (t, J = 7.5 Hz, 2H), 3.92 (s, 3H), 4.00 (s, 3H), 5.19 (br s, 1H), 6.42 (s, 1H); ESI-MS (*m*/*z*) 391 $[M + H]^+$. ^{13}C-UST: ^{1}H NMR (300 MHz, $CDCl_3$) δ 0.88 (t, J = 6.4 Hz, 3H), 1.21−1.42 (m, 16H), 1.73 (tt, J = 7.5, 7.5 Hz, 2H), 2.00 (d, $^3J_{CH}$ = 3.6 Hz, 3H), 2.67 (t, J = 7.4 Hz, 2H), 3.93 (s, 3H), 4.00 (s, 3H), 5.14 (br s, 1H), 6.43 (s, 1H); ESI-MS (*m*/*z*) 392 $[M + H]^+$.

Sample Preparation. The cytochrome bc_1 complex was prepared as described (*19*) and eluted from the HyperD DEAE column after detergent exchange in buffer: 300 mM NaCl, 50 mM KP_i (pH 6.9), and 0.05% UM. This buffer was used in the electrochemical and spectroscopic studies. The inhibitors were added at a final concentration of 1 μM or substoichiometric to the cytochrome bc_1 complex (final concentration of 0.3−0.5 mM). Activity assays were per-

formed as described (*19*). UST is a less potent inhibitor than natural stigmatellin in the case of the *S. cerevisiae* bc_1 complex. Under the given assay conditions a 10-fold molar excess of inhibitor to enzyme is necessary to obtain more than 10% inhibition of WT activity. The inhibitory potency in terms of IC_{50} value of UST with the bovine bc_1 complex is 4.0 nM (H. Miyoshi, unpublished results).

Electrochemistry. The ultrathin layer spectroelectrochemical cell was used as previously described (*20*, *21*). Experiments of the ethanol-soluble UST were performed in CH_3OD, with tetrabutylammonium hexafluorophosphate as electrolyte and a pseudoreference (an electrode consisting of a platinum wire in a CH_3OD solution containing UST and tetrabutylammonium hexafluorophosphate).

For experiments with proteins, the gold grid working electrode was modified with a mixture of 2 mM solutions of cysteamine and mercaptopropionic acid for 1 h and then washed with deionized water to avoid irreversible protein adhesion, as previously described in ref *16*. To accelerate the redox reactions, a mixture of 17 mediators (see ref *16*, except diethyl-3-methyl-*p*-phenylenediamine and dimethyl-*p*-phenylenediamine, but adding quinhydrone) was added in a substoichiometric concentration of 40 μM to the protein solution; 7−8 μL of the solution was used to fill the electrochemical cell. The cell path length was below 10 μm, as determined at the beginning of each experiment. All experiments were performed at 278 K. Potentials were obtained vs Ag/AgCl and are given with respect to the standard hydrogen electrode (SHE′) at pH 7 in the study.

Spectroscopy. FTIR and UV/vis difference spectra were simultaneously recorded as a function of the applied potential using a setup combining an IR beam from the interferometer (modified IFS 25; Bruker, Germany) for the 4000−1000 cm^{-1} range and a dispersive spectrometer for the 400−900 nm range as reported previously (*20*). First, the protein was equilibrated at an initial electrode potential, and a single-beam spectrum was recorded. Then the final potential was applied, and a single-beam spectrum was again recorded after equilibration. Equilibration generally took less than 4 min for the full potential step from −0.292 to +0.708 V as followed by the difference signals in the visible spectral range (not shown). Infrared difference spectra as presented here were calculated from two single-beam spectra, with the initial spectrum taken as reference. Typically, 128 interferograms at 4 cm^{-1} resolution were summed for each single-beam spectrum and Fourier transformed using triangular apodization and a zero filling factor of 2. In general, 8−10 difference spectra were averaged.

RESULTS AND DISCUSSION

Synthesis of Undecylstigmatellin. The molecular structures of natural stigmatellin A and [4-^{13}C]undecylstigmatellin (UST) are shown in Figure 1. Both compounds are potent inhibitors of ubiquinol oxidation, and on the basis of structural resemblance, UST is expected to bind in a manner similar to that of the ubiquinol. Thierbach et al. (*32*) showed that the natural side chain is not essential for potent inhibition and can be substituted by a long alkyl chain. In a similar manner, decylubiquinone is readily used for determination of catalytic activity of the enzyme.

Electrochemically Induced FTIR Difference Spectra of the S. cerevisiae bc_1 Complex. The electrochemically induced

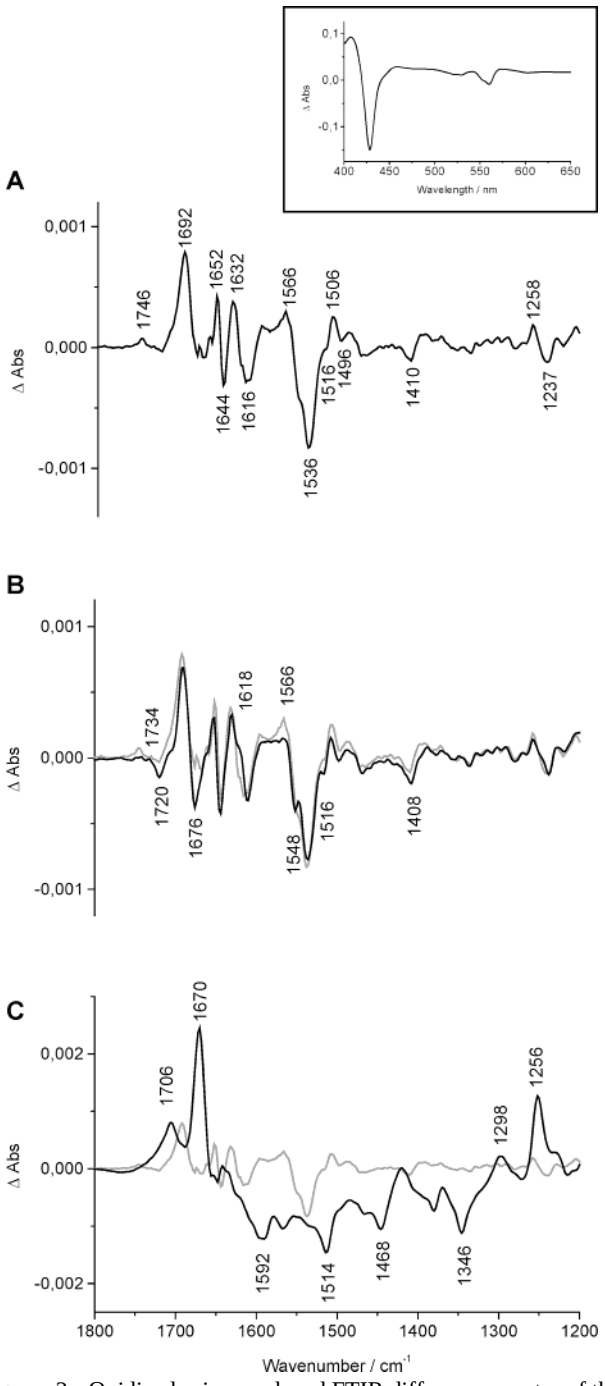

FIGURE 2: Oxidized-minus-reduced FTIR difference spectra of the wild-type *S. cerevisiae* bc_1 complex (A). Oxidized-minus-reduced FTIR difference spectra obtained in the presence of a (B) 1 μM or substoichiometric amount of natural stigmatellin A (black, full line) and (C) 10 μM inhibitor (black, full line) in direct comparison to WT (gray line, panels B and C) for a potential step from −0.292 to 0.708 V (vs SHE′). The inset shows the oxidized-minus-reduced visible difference spectra as typically monitored to control the full reaction of the enzyme.

FTIR difference spectra of the bc_1 complex from *S. cerevisiae* for a potential step from −0.292 to 0.708 V in the spectral range from 1800 to 1000 cm^{-1} are presented in Figure 2. The inset presents a typical oxidized-minus-reduced visible difference spectrum recorded to monitor the redox state of the enzyme. In the oxidized-minus-reduced FTIR difference spectra positive bands represent signals associated with the oxidized state of the protein and negative signals with the reduced state. Generally, in the given spectral range, signals

from conformational changes of the protein backbone and the cofactors are expected, as well as protonation/deprotonation reactions and conformational changes of the amino acid side chains. Overall, the spectra contain a significant number of overlapping bands. Three main regions can be distinguished: the 1690−1620 cm^{-1} region (amide I), the 1560−1520 cm^{-1} region (amide II), and the region from 1100 to 1000 cm^{-1}, where contributions of the phosphate buffer dominate the spectrum.

In the amide I range, modes from the ν(C═O) stretch vibrations of the polypeptide backbone are expected, and absorptions characteristic for the different secondary structure elements can be discriminated (*22*). Several bands are seen in the amide I region. Whereas the band at 1692 and 1632 cm^{-1} may involve β-sheet elements, the peak at 1652 cm^{-1} includes signals from the predominantly α-helical structure of the enzyme. In addition, the ν(C═O) modes of the bound quinones are expected in the spectra. On the basis of comparison to model compounds and recent FTIR studies of other bc_1 complexes, an involvement in the vibrational modes between 1650 and 1630 cm^{-1} is likely (*14*, *17*, *18*, *23*). Further signals for the bound neutral quinone(s) can be expected at 1610 cm^{-1} [ν(C═C)] and 1264 cm^{-1} [δ(C−OCH_3], while the negative signals at approxomately 1490, 1470, 1432, and 1388 cm^{-1} include contributions from the reduced and protonated quinol forms (*24*). In the bc_1 complex preparation used here, the natural substrate UQ6 is bound at the Q_i site as shown in the crystal structures (*2*, *33*). In comparison to the FTIR spectra obtained with the same method for the bacterial bc_1 complex from *Pseudomonas denitrificans* (*17*), a significantly smaller contribution from quinol/quinone signals is observed here, pointing to less quinol content of this protein preparation. Especially, the prominent signal at 1656 cm^{-1}, tentatively assigned to the Q_o site for the bc_1 complex from *P. denitrificans*, is absent here, suggesting that the Q_o site is not occupied in the wild-type *S. cerevisiae* preparation.

On the basis of previous studies signals from the three hemes, b_L, b_H, and c_1, including the heme propionates, vinyl side chains, and the porphyrin ring, are expected. On the basis of heme model studies, the strong positive signal at 1692 cm^{-1} is likely to include ν(C═O) modes of protonated heme propionates (*25*). The modes characteristic for deprotonated heme propionates in cytochrome *c* oxidase were determined by specific ^{13}C labeling at the propionates and attributed in the range from 1570 to 1530 cm^{-1} to the antisymmetric COO^- vibration (*26*). Therefore, the signal at 1566 cm^{-1} is tentatively assigned to this vibration, whereas a possible candidate for the symmetric COO^- vibration can be found at 1410 cm^{-1}. Structural analysis assigned a crucial role to the heme b_L propionate A in the proposed proton exit pathway at the Q_o site (see refs *2* and *33*). In this model, a coupled electron−proton transfer toward the heme b_L propionate A is suggested. Upon rotational displacement away from the Q_o site, the side chain of Glu272 is hydrogen bonded via a single water molecule to propionate A (*33*), which is hydrogen bonded to Arg79. From Arg79, there is a defined hydrogen bond network to outside, including stabilizing residues Glu66 and Arg70, and several water molecules (*33*). On this basis the involvement of heme propionate modes in the redox-induced FTIR difference spectra is most likely.

Heme ν(C═C) modes of the porphyrin ring are typically involved in the broad mode between 1550 and 1530 cm^{-1}. However, some involvement of the coupled CN stretching and NH bending modes of the backbone, the so-called amide II mode, is also expected in this spectral region. Signals from the Rieske [2Fe-2S] cluster cannot be found in the investigated spectral range, because the Fe−S vibration mode is present at lower frequencies. However, alterations of the backbone and amino acid side chains of the direct cluster environment may contribute to the spectrum. The amide I and II modes derived from the backbone contain information about the conformational change described by the *ef*-loop displacement as response to Q_o site occupancy (see refs *30* and *33*).

The spectral region above 1710 cm^{-1} is characteristic for protonated aspartic or glutamic acids. Clearly a peak at 1746 cm^{-1} is present, reflecting the contribution of an aspartic or glutamic acid protonated in the oxidized form. For the deprotonated form signals between 1590 and 1540 cm^{-1} are expected for the $(COO^-)^{as}$ mode and between 1420 and 1370 cm^{-1} for the $(COO^-)^{s}$ mode.

Another interesting residue, tyrosine, is known to contribute to infrared spectra, with significant extinctions, i.e., with the ν_{19}(CC) ring mode at approximately 1518 cm^{-1}. For deprotonated tyrosine the ν_{19}(CC) ring mode is expected at approximately 1499 cm^{-1}, reflecting the sensitivity of the ring modes to the protonation state of the phenol group. The $\nu_{7'a}$(CO) mode is present at approximately 1269 cm^{-1}, but the exact position depends on the hydrogen bond environment (*27*−*28*). In the data presented for the bc_1 complex so far, differential signals at 1496/1516 cm^{-1} are tentatively attributed to the rearrangement and/or protonation of tyrosines upon the redox reaction. Tyr279 has been suggested to be crucial for positioning of the substrate ubiquinol in the active site. In addition, Tyr132 and Tyr274 are part of the suggested proton pathway (*2*, *35*). Clear assignments for all mentioned side chains need support by site-directed mutagenesis.

Electrochemically Induced FTIR Difference Spectra of the S. cerevisiae bc_1 Complex in the Presence of Stigmatellin A. The effect of stigmatellin A binding on the electrochemically induced FTIR difference spectra is presented in Figure 2B for a substoichiometric amount of natural stigmatellin A (black, full line), in direct comparison to the wild-type spectrum (gray line). Clear variations can be seen upon binding of a substoichiometric amount of stigmatellin for the full spectral range displayed. Intensity shifts in the amide I range between 1690 and 1676 cm^{-1}, perturbations in the spectral regions between 1620 and 1400 cm^{-1}, and distinct changes in the region between 1720 and 1750 cm^{-1}, where protonated acidic groups absorb, were observed. These shifts may be attributed to (i) variations in the protein upon inhibitor binding but, importantly, also to (ii) the inhibitor itself. In the latter case, stigmatellin should be redox active, because the signals are obtained from redox-induced FTIR difference spectra. To probe this suggestion, spectra of the enzyme with a 10-fold increase of stigmatellin added, were measured (Figure 2C). The signals seen in Figure 2C reveal the increase of several signals that exclusively arise upon increased stigmatellin content. Due to the fact that inhibitor-specific modes were observed in the spectra, stigmatellin has to be regarded as a redox-active compound. We note that

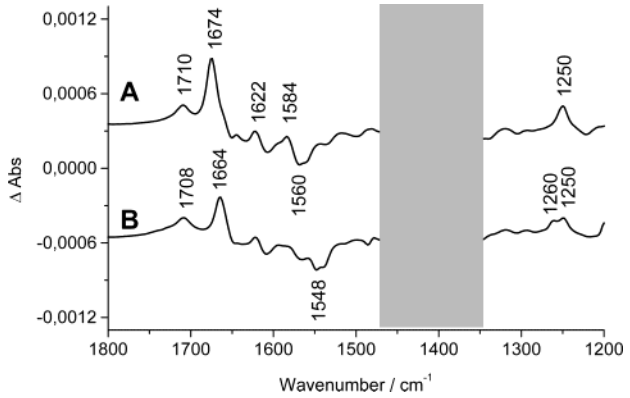

FIGURE 3: Oxidized-minus-reduced FTIR difference spectra of ^{12}C-UST (A) and ^{13}C-UST (B) as obtained in CH_3OD for a potential step from −0.272 to 0.708 V (vs SHE′). Due to the strong absorbance of the solvent, the spectral region from 1470 to 1350 cm^{-1} is disregarded.

the final concentration of inhibitor was in all further experiments substoichiometric, i.e., 0.3−0.5 mM enzyme vs micromolar inhibitor.

To discriminate protein-specific variations model compound studies in solvent and experiments with a newly synthesized stigmatellin derivative were performed. The studies with labeled (4-^{13}C═O) and unlabeled compounds, described below, led to a more detailed understanding of the electrochemically induced FTIR difference spectra.

Electrochemically Induced FTIR Difference Spectra of the UST in CH_3OD. Figure 3 shows the electrochemically induced FTIR difference spectra of ^{12}C-UST (A) and ^{13}C-UST (B) as obtained in CH_3OD for a potential step from −0.292 to 0.708 V vs SHE′. Due to the strong absorption of the solvent between 1480 and 1300 cm^{-1}, this spectral region is not shown. The positive signals in Figure 3 correlate with the oxidized form of the inhibitors and can also be found in the absorbance spectra obtained (data not shown). The negative signals reflect the reduced form of the inhibitors. The difference spectrum obtained for the bc_1 complex when stigmatellin concentration was increased (Figure 2C, black line) corresponds to the UST in solution, confirming that the stigmatellin contributes in the redox-induced FTIR difference spectra and is electrochemically active.

Briefly, the spectral region between 1720 and 1650 cm^{-1} includes the ν(C═O) vibrational modes, as well as the ν-(C═O) modes coupled to the ν(C═C) ring modes. In the region between 1640 and 1500 cm^{-1} the ν(C═C) vibrational modes of the rings are found, whereas the δ(OH) vibration is expected below 1400 cm^{-1}. Assuming a completely uncoupled vibration, ^{13}C labeling at the carbonyl carbon could induce a shift of up to 35 cm^{-1} (*29*). For the molecule studied here, however, we may clearly expect a vibration coupled to the ring modes, leading to the observed shift of 10 cm^{-1} for the ν(C═O) vibrational mode. In addition, an effect on the ν(C═C/C−C) ring modes was expected. The data presented here showed that, besides the shift of the ν-(C═O) vibration from 1674 to 1664 cm^{-1} (Figure 3) and small variations at 1710 cm^{-1}, a shift of the ν(C═C/C−C) modes at 1570−1560 cm^{-1} to 1548−1536 cm^{-1} was observed in the difference spectra upon ^{13}C labeling at the 4-position. Bands derived from the possible formation of a C4-OH group upon reduction of UST might be buried below

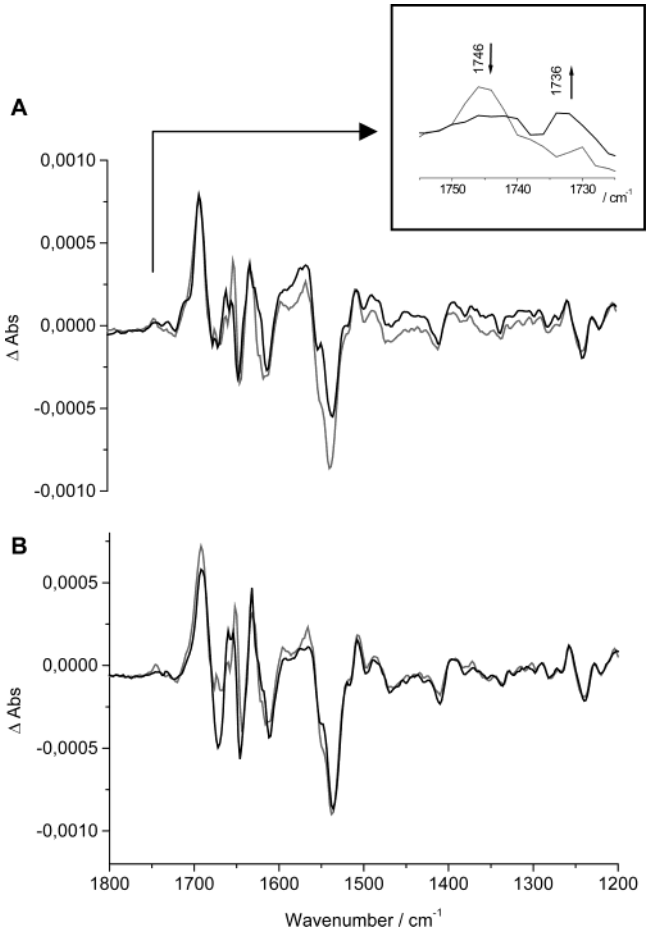

FIGURE 4: Electrochemically induced FTIR difference spectra of the *S. cerevisiae* bc_1 complex in the presence of (A) UST and (B) ^{13}C-UST (black line) in direct comparison to WT (gray line). The inset shows the enlarged view of the spectral range from 1755 to 1725 cm^{-1}, the signals having a maximum intensity of 1×10^{-4} OD.

the CH_3OD absorbance. In the lower spectral region, a signal was relocated from 1250 to 1264 cm^{-1}, probably as a result of a ring (C−C/C═C) or δ(C−O) vibration, perturbed upon labeling.

Electrochemically Induced FTIR Difference Spectra of the S. cerevisiae bc_1 Complex in the Presence of UST and ^{13}C-UST. Electrochemically induced FTIR difference spectra of the *S. cerevisiae* bc_1 complex in the presence of UST (A) and ^{13}C-UST (B) in direct comparison to wild type (gray line) are shown in Figure 4. Pronounced variations are observed in the full spectral range from 1800 to 1200 cm^{-1}. Both the redox-dependent contributions of the inhibitor and reorganizations within the protein contribute to the spectra. In addition, contributions from unbound inhibitor were expected. To distinguish between these contributions, two different comparisons were made on the basis of double difference spectra calculated from the data shown in Figures 2 and 4. Figure 5A shows the double difference spectra obtained by subtracting the redox-induced FTIR difference spectra of ^{12}C- to ^{13}C-UST bound to the protein. In Figure 5B the ^{13}C sensitive modes were distinguished by subtracting the spectra of ^{12}C- to ^{13}C-UST in solution. (Figure 5B). Furthermore, the effect of inhibitor binding was demonstrated by subtracting of the WT spectrum from the data where the inhibitor is bound in Figure 6.

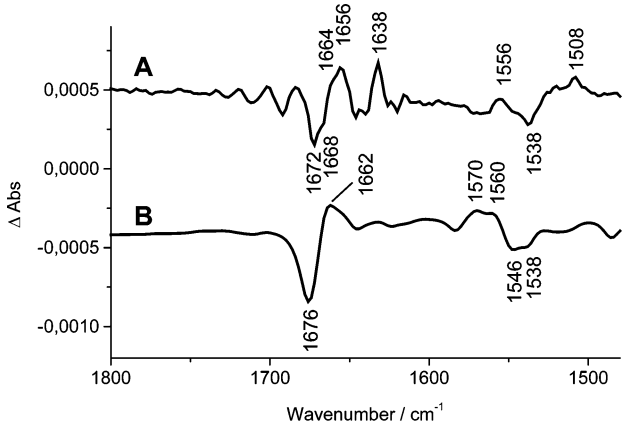

FIGURE 5: Effect of the ^{13}C labeling depicted in a double difference spectrum calculated from the UST minus ^{13}C-UST spectra as bound to the protein (A) and in solution (B).

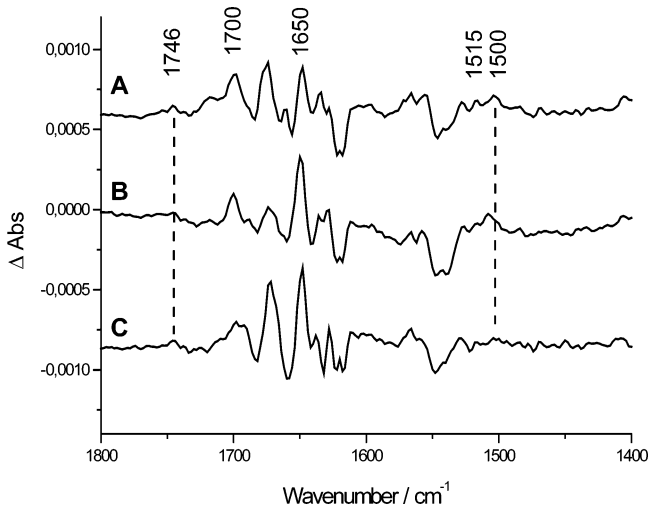

FIGURE 6: Double difference spectrum reflecting the stigmatellin binding as obtained by subtracting WT from the spectra with stigmatellin (A) and by subtracting WT from the data with ^{12}C-UST (B) vs WT minus ^{13}C-UST (C).

The ^{13}C sensitive shifts (Figure 5B) include the differential mode of the ν(C═O) vibration of the oxidized form from 1676 to 1662 cm^{-1}. In the protein-bound form (Figure 5A) the analogous signal is seen at 1672 cm^{-1} with a shoulder at 1668 cm^{-1} and at 1656 cm^{-1} with a shoulder at 1664 cm^{-1}. Since some of the inhibitor is not bound, we attribute the signal at 1672 cm^{-1} to the unbound inhibitor and the signal at 1668 cm^{-1} to the bound ^{12}C═O group. For the ^{13}C═O the shoulder at 1664 cm^{-1} seems to arise from the unbound form and the signal at 1656 cm^{-1} from the bound form. The ν(C═O) vibration of the UST molecule obviously experiences a shift of 8 cm^{-1} upon binding to the protein, the lower frequency indicating a hydrogen bond to the carbonyl group, consistent with the structural information, where His181 of ISP and the C4-carbonyl group are positioned in favorable geometry for forming a hydrogen bond (*2*). Also, in the spectral range between 1580 and 1530 cm^{-1} a ^{13}C═O sensitive change is observed. The modes at 1570 and 1560 cm^{-1} shift to 1546 and 1538 cm^{-1}. In the protein-bound form, a differential signal at 1556 and 1538 cm^{-1} can be depicted. Shifts of up to 14 cm^{-1} reflect the stabilization of the inhibitor ring system, the ring modes being strongly coupled to the ν(C═O) vibration, as concluded above. In addition to the strong polar interactions to His181 and Glu272 (Figure 7), multiple stabilizing interactions from the cytochrome *b* subunit residues with the chromone ring system were observed in the structure, including numerous van der Waals interactions and weak hydrogen bonds (*2*).

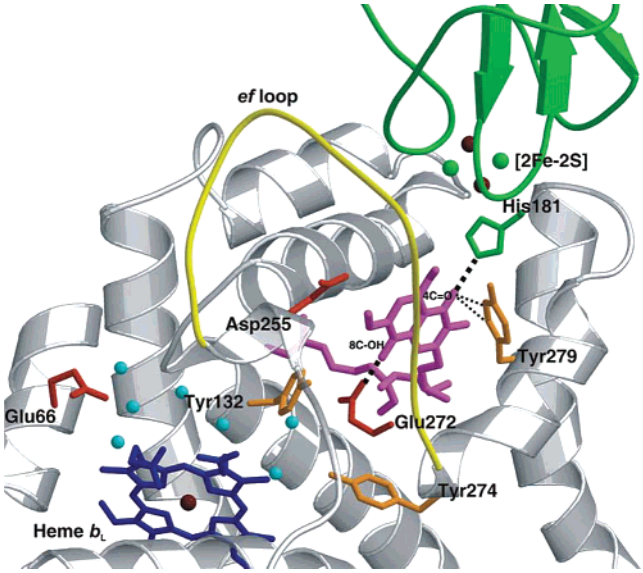

FIGURE 7: The Q_o site viewed from the intermembrane space. Cytochrome *b* (secondary structure elements shown in gray) forms the crater into which the [2Fe-2S] cluster-bearing tip of the Rieske (green) docks. Stigmatellin (magenta) binding is stabilized by hydrogen bonds (dotted lines) to His181 and Glu272, which have been suggested to act as primary quinol ligands and proton acceptors. Acidic residues and tyrosines discussed in the text are depicted in red and orange, respectively. Structural water molecules on the proposed proton exit pathway via heme b_L propionate A are shown as cyan spheres. The catalytically important and conformationally flexible *ef* loop of cytochrome *b* provides a lid on the Q_o site and is depicted in yellow. The figure is generated from the yeast bc_1 complex (PDB entry 1KB9) using Molscript (*34*) and Raster3D (*35*).

On the basis of the double difference spectra seen the signals concomitant with ^{12}C-UST (B) and ^{13}C-UST (C) binding to the protein can be distinguished in Figure 6. Clearly, changes are present in the spectral region characteristic for protonated acidic residues between 1670 and 1780 cm^{-1}. As described above signals from protonated heme propionates are expected between 1670 and 1700 cm^{-1}, whereas protonated aspartic and glutamic acid side chains are exclusively observed at modes higher than 1710 cm^{-1}. The mode at 1746 cm^{-1} is clearly decreased upon UST binding, demonstrating the deprotonation of an aspartic or glutamic acid upon binding. Additionally, the increase of a small mode at 1736 cm^{-1} is observed (see insert to Figure 4 and Figure 6). Alternatively, the conformational rearrangement of a protonated residue may be inducing a shift from 1746 to 1736 cm^{-1}.

The mode shifted at 1700 cm^{-1} is within the spectral range of a protonated heme propionate, perturbed upon stigmatellin binding. The mode for the deprotonated form of the acidic groups may be involved in the differential signals between 1570 and 1530 cm^{-1}; however, the modes from the inhibitor are partially overlapping in the region, and a clear discrimination is difficult.

Tyrosines are found to demonstrate clear signals at approximately 1500 and 1515 cm^{-1}, depending on protona-

tion state and hydrogen-bonding environment (*27*). We suggest that the rearrangements and possible protonation reactions at 1500 and 1515 cm^{-1} arise from tyrosines perturbed upon stigmatellin binding. Structural analysis has shown the repositioning of the Tyr279 side chain upon substrate binding (*30*) and subsequent formation of two weak hydrogen bonds (C−H···O═C), which are suggested to contribute to stabilization of the ligand in the binding site (*33*) (Figure 7). Other tyrosines of structural/functional relevance include Tyr132 and Tyr274, which serve as stabilizing residues in the suggested proton pathway (*2*) and are depicted in Figure 7. A final attribution for the mentioned side chains need support by site-directed mutagenesis.

Further reorganizations upon stigmatellin binding are expected in the amide I and II region that must contain information about the conformational change described by the *ef*-loop displacement as response to Q_o site occupancy (see refs *30* and *33*). In the double difference spectra seen in Figure 6, signals are present between 1690 and 1615 cm^{-1} in the amide I region and around 1550 cm^{-1} in the amide II region. The signal at 1668 cm^{-1} includes contributions of the ν(C═O) mode from the stigmatellin itself; however, it is not fully shifted upon ^{13}C═O labeling. It may additionally include backbone reorganizations at a position typical for turns and loops. The mode at 1650 cm^{-1} may display variations at unordered elements or at α-helical components. Signals at 1634 and 1617 cm^{-1} are present at positions that account for β-sheet secondary structure elements (*22*). When structures of the native and inhibited enzymes are compared, the "fixing" of the Rieske extrinsic domain (β-sheet and turns) and displacement of the *ef* and *cd* loops to accommodate the Q_o site occupant are the major conformational changes observed (*2*, *30*).

CONCLUSIONS

In this work we could monitor the binding of stigmatellin and its derivatives to the bc_1 complex from *S. cerevisiae* by electrochemically induced FTIR difference spectroscopy. The comparison of spectra obtained from wild type and the bc_1 complex inhibited with natural stigmatellin A, ^{12}C- and ^{13}C-UST, allowed the assignment of protein-specific features upon inhibitor binding. Interestingly, the inhibitors were found to be redox active, and assignment of bands derived from stigmatellin itself was carried out. The highly coupled ν(C═O) mode was identified on the basis of ^{13}C labeling of the carbonyl group. Importantly, these observations show that the coreduction of the inhibitor has to be regarded in studies where reduction of the enzyme in the presence of inhibitor is monitored. In case the carbonyl (C═O) group of stigmatellin is reduced to a hydroxyl (OH) group, the interaction with the protein needs to be reevaluated from a functional point of view, since the highly discussed interaction of His181 would have to take place via the oxygen atom of the OH group. Further studies on the reduced form of the inhibitor will have to clarify the structure of the reduced stigmatellin molecule.

In the electrochemically induced FTIR difference spectra obtained for the binding of the inhibitors, several signals could be attributed to variations occurring upon binding of the inhibitors to the protein. Interestingly, a signal at 1746 cm^{-1} decreases upon stigmatellin binding whereas a signal at 1736 cm^{-1} arises (see insert to Figure 4). These signals are located in a spectral region that exclusively includes contributions from protonated acidic groups, providing evidence that the binding of the inhibitor affects one or two protonated side chains. To interpret these spectral changes, two different scenarios can be considered. One explanation could be that the binding of inhibitor induces an environmental change of a protonated residue, leading to weaker hydrogen bonding and inducing the downshift of the ν(C═O) vibrational mode. Alternatively, the decrease in signal at 1746 cm^{-1} could be explained as deprotonation of an acidic residue, whereas the emerging signal at 1736 cm^{-1} would be derived from protonation of another residue.

Figure 7 shows the binding of stigmatellin at the Q_o site, and protonable residues are pointed out. Glu272 was shown to be a direct interaction partner to the hydroxyl group of stigmatellin (*2*, *35*) and thus was suggested to be deprotonated. When rotated away from the empty Q_o site, Glu272 was proposed to be deprotonated and stabilized by hydrogen bonds to protonated residues, such as His253 and Tyr274 (*33*). The rotation of Glu272 into the binding pocked led to the proposed role of this residue as a quinol ligand and primary proton acceptor in quinol oxidation. Upon rotational displacement of its side chain, it could deliver the proton via a hydrogen-bonded water molecule and the heme b_L propionate A to the outside (*33*).

Assuming Glu272 to be protonated also in the inhibitor-bound form of the oxidized enzyme, both signals in the infrared data, the mode at 1746 cm^{-1} for the free binding site and the mode at 1736 cm^{-1} for the occupied site, would be derived from Glu272. This suggestion, however, is not in line with the role of Glu272 as the proton acceptor and primary ligand of ubiquinol. In the alternative explanation, a different residue has to be considered to be perturbed upon binding, for example, Glu66 or Asp255, highlighted in Figure 7. Importantly, this FTIR spectroscopic study clearly demonstrated that a minimum of one protonated aspartic or glutamic acid side chain is involved in the binding of stigmatellin to the cytochrome bc_1 complex from *S. cerevisiae*.

In addition to the spectral range characteristic for protonated acidic residues, also the interaction of the inhibitor with other residues is detectable. Briefly, the mode shifted at 1700 cm^{-1} is clearly within the spectral range of a protonated heme propionate perturbed upon stigmatellin binding. Variations from amide modes indicated conformational changes of the backbone upon inhibitor binding. Other protein-specific signals in the spectra are derived from amino acid side chains such as tyrosines, arginines, asparagines, and glutamines. As mentioned above, Tyr132, Tyr274, and Tyr279 are the likely candidates for reorganizations in the redox-induced FTIR difference spectra, tyrosines typically contributing at 1500 and 1515 cm^{-1}. A final assignment of the interacting side chains will be performed in combination with site-directed mutagenesis in future studies.

REFERENCES

1. Berry, A. B., Guergova-Kuras, M., Huang, L., and Crofts, A. R. (2000) Structure and function of cytochrome *bc* complexes, *Annu. Rev. Biochem. 69*, 1005−1075.
2. Hunte, C., Koepke, J., Lange, C., Rossmanith, T., and Michel, H. (2000) Structure at 2.3 Å resolution of the cytochrome bc_1 complex

from the yeast *Saccharomyces cerevisiae* cocrystallized with an antibody Fv fragment, *Structure 8*, 669−684.
3. Iwata, S., Lee, J. W., Okada, K., Lee, J. K., Iwata, M., Rasmussen, B., Link, T. A., Ramaswamy, S., and Jap, B. K. (1998) Complete structure of the 11-subunit bovine mitochondrial cytochrome bc_1 complex, *Science 281*, 64−71.
4. Zhang, Z., Huang, L., Shulmeister, V. M., Chi, Y., Kim, K. K., Hung, L. W., Crofts, A. R., Berry, E. A., and Kim, S. H. (1998) Electron transfer by domain movement in cytochrome bc_1, *Nature 392*, 677−684.
5. Xia, D., Yu, C. A., Kim, H., Xia, J. Z., Kachurin, A. M., Zhang, L., Yu, L., and Deisenhofer, J. (1997) Crystal structure of the cytochrome bc_1 complex from bovine heart mitochondria, *Science 277*, 60−66.
6. Mitchell, P. (1976) Possible molecular mechanisms of the protonmotive function of cytochrome systems, *J. Theor. Biol. 62*, 327−367.
7. Trumpower, B. L. (1990) The protonmotive Q cycle. Energy transduction by coupling of proton translocation to electron transfer by the cytochrome bc_1 complex, *J. Biol. Chem. 265*, 11409−11412.
8. Brandt, U., and Trumpower, B. (1994) The protonmotive Q cycle in mitochondria and bacteria, *Crit. Rev. Biochem. Mol. Biol. 29*, 165−197.
9. Crofts, A. R., and Wang, Z. (1989) How rapid are the internal reactions of ubiquinol: cytochrome c_2-oxidoreductase?, *Photosynth. Res. 22*, 69−87.
10. Link, T. A. (1997) The role of the "Rieske" iron sulfur protein in the hydroquinone oxidation (Q(P)) site of the cytochrome bc_1 complex. The "proton-gated affinity change" mechanism, *FEBS Lett. 412*, 257−264.
11. Brandt, U. (1996) Bifurcated ubihydroquinone oxidation in the cytochrome bc_1 complex by proton-gated charge transfer, *FEBS Lett. 387*, 1−6.
12. Ding, H., Moser, C. C., Robertson, D. E., Tokito, M. K., Daldal, F., and Dutton, P. L. (1995) Ubiquinone pair in the Q_o site central to the primary energy conversion reactions of cytochrome bc_1 complex, *Biochemistry 34*, 15979−15996.
13. Sharp, R. E., Gibney, B. R., Palmitessa, A., White, J. L., Dixon, J. A., Moser, C. C., Daldal, F., and Dutton, P. L. (1999) Effect of inhibitors on the ubiquinone binding capacity of the primary energy conversion site in the *Rhodobacter capsulatus* cytochrome bc_1 complex, *Biochemistry 38*, 14973−14980.
14. Baymann, F., Robertson, D. E., Dutton, P. L., and Mäntele, W. (1999) Electrochemical and spectroscopic investigations of the cytochrome bc_1 complex from *Rhodobacter capsulatus*, *Biochemistry 38*, 13188−13199.
15. Hellwig, P., Behr, J., Ostermeier, C., Richter, O. M., Pfitzner, U., Odenwald, A., Ludwig, B., Michel, H., and Mäntele, W. (1998) Involvement of glutamic acid 278 in the redox reaction of the cytochrome *c* oxidase from *Paracoccus denitrificans* investigated by FTIR spectroscopy, *Biochemistry 37*, 7390−7399.
16. Hellwig, P., Scheide, D., Bungert, S., Mäntele, W., and Friedrich, T. (2000) FT-IR spectroscopic characterization of NADH:ubiquinone oxidoreductase (complex I) from *Escherichia coli*: oxidation of FeS cluster N2 is coupled with the protonation of an aspartate or glutamate side chain, *Biochemistry 39*, 10884−10891.
17. Ritter, M., Anderka, O., Ludwig, B., Mäntele, W., and Hellwig, P. (2003) Electrochemical and FTIR spectroscopic characterization of the cytochrome bc_1 complex from *Paracoccus denitrificans*: evidence for protonation reactions coupled to quinone binding, *Biochemistry 42*, 12391−12399.
18. Iwaki, M., Giotta, L., Akinsiku, A. O., Schägger, H., Fisher, N., Breton, J., and Rich, P. R. (2003) Redox-induced transitions in bovine cytochrome bc_1 complex studied by perfusion-induced ATR-FTIR spectroscopy, *Biochemistry 42*, 11109−11119.
19. Palsdottir, H., and Hunte, C. (2003) Purification of the cytochrome bc_1 complex from yeast, in *Membrane Protein Purification and Crystallization—A practical guide* (Hunte, C., von Jagow, G., and Schagger, H., Eds.) 2nd ed., Academic Press and Elsevier Science, New York.
20. Moss, D., Nabedryk, E., Breton, J., and Mäntele, W. (1990) Redox-linked conformational changes in proteins detected by a combination of infrared spectroscopy and electrochemistry: Evaluation of the technique with cytochrome *c*, *Eur. J. Biochem. 187*, 565−572.
21. Mäntele, W. (1993) Reaction-induced infrared difference spectroscopy for the study of protein function and reaction mechanisms, *Trends Biochem. Sci. 18*, 197−202.
22. Goormaghtigh, E., Cabiaux, V., and Ruysschaert, J. M. (1994) Determination of soluble and membrane protein structure by Fourier transform infrared spectroscopy. III. Secondary structures, *Subcell. Biochem. 23*, 405−450.
23. Breton, J., Burie, J. R., Berthomieu, C., Berger, G., and Nabedryk, E. (1994) The binding sites of quinones in photosynthetic bacterial reaction centers investigated by light-induced FTIR difference spectroscopy: assignment of the QA vibrations in *Rhodobacter phaeroides* using ^{18}O- or ^{13}C-labeled ubiquinone and vitamin K1, *Biochemistry 33*, 4953−4965.
24. Hellwig, P., Mogi, T., Tomson, F. L., Gennis, R. B., Iwata, J., Miyoshi, H., and Mäntele, W. (1999) Vibrational modes of ubiquinone in cytochrome bo_3 from *Escherichia coli* identified by Fourier transform infrared difference spectroscopy and specific ^{13}C labeling, *Biochemistry 38*, 14683−14689.
25. Berthomieu, C., Boussac, A., Mäntele, W., Breton, J., and Nabedryk, E. (1992) Molecular changes following oxidoreduction of cytochrome b_{559} characterized by Fourier transform infrared difference spectroscopy and electron paramagnetic resonance: photooxidation in photosystem II and electrochemistry of isolated cytochrome b_{559} and iron protoporphyrin IX-bisimidazole model compounds, *Biochemistry 31*, 11460−11471.
26. Behr, J., Hellwig, P., Mäntele, W., and Michel, H. (1998) Redox dependent changes at the heme propionates in cytochrome *c* oxidase from *Paracoccus denitrificans*: direct evidence from FTIR difference spectroscopy in combination with heme propionate ^{13}C labeling, *Biochemistry 37*, 7400−7406.
27. Venyaminov, S. Y., and Kalnin, N. N. (1990) Quantitative IR spectrophotometry of peptide compounds in water (H2O) solutions. I. Spectral parameters of amino acid residue absorption bands, *Biopolymers 30*, 1243−1257.
28. Hienerwadel, R., Boussac, A., Breton, J., Diner, B. A., and Berthomieu, C. (1997) Fourier transform infrared difference spectroscopy of photosystem II tyrosine D using site-directed mutagenesis and specific isotope labeling, *Biochemistry 36*, 14712−14723.
29. Herzberg, G. (1962) Isotope effects, in *Molecular spectra and molecular structure: II. Infrared and Raman spectra of polyatomic molecules*, Chapter 6, pp 227−238, van Nostrand, Princeton, NJ.
30. Crofts, A. R., Barquera, B., Gennis, R. B., Kuras, R., Guergova-Kuras, M. and Berry, E. A. (1999) Mechanism of ubiquinol oxidation by the bc_1 complex: different domains of the quinol binding pocket and their role in the mechanism and binding of inhibitors, *Biochemistry 38*, 15807−15826.
31. Enders, D., Geibel, G., and Osborne, S. (2000) Diastereo- and enantioselective total synthesis of stigmatellin A, *Chem. Eur. J. 6*, 1302−1309.
32. Thierbach, G., Kunze, B., Reichenbach, H., and Höfle, G. (1984) The mode of action of stigmatellin, a new inhibitor of the cytochrome bc_1 segment of the respiratory chain, *Biochim. Biophys. Acta 765*, 227−235.
33. Palsdottir, H., Lojero, C. G., Trumpower, B. L., and Hunte, C. (2003) Structure of the yeast cytochrome bc_1 complex with a hydroxyquinone anion Q_o site inhibitor bound, *J. Biol. Chem. 278*, 31303−31311.
34. Kraulis, P. J. (1991) MOLSCRIPT: a program to produce both detailed and schematic plots of protein structures, *J. Appl. Crystallogr. 24*, 946−950.
35. Merritt, E. A., and Murphy, M. E. P. (1994) Raster3D Version 2.0. A program for photorealistic molecular graphics, *Acta Crystallogr. D50*, 869−873.

BI049649X